

Impact of horizontal resolution and model time step on European precipitation extremes in the OpenIFS 43r3 atmosphere model

Yingxue Liu^{1,2}, Joakim Kjellsson^{1,2}, Abhishek Savita¹ and Wonsun Park^{3,4}

¹GEOMAR Helmholtz Centre for Ocean Research Kiel, Kiel, Germany

²Faculty of Mathematics and Natural Sciences, Christian Albrechts University of Kiel, Kiel, Germany

³Center for Climate Physics, Institute for Basic Science (IBS), Busan, Republic of Korea

⁴Department of Integrated Climate System Science, Pusan National University, Busan, Republic of Korea

Correspondence to: Yingxue Liu (yiliu@geomar.de)

Abstract: Events of extreme precipitation pose a hazard to many parts of Europe but are typically not well represented in climate models. Here, we evaluate daily extreme precipitation over Europe during 1982–2019 in observations (GPCC), reanalysis (ERA5) and a set of atmosphere-only simulations at low- (100 km), medium- (50 km) and high- (25 km) horizontal resolution and also at different time steps (i.e., 60, 30 and 15 min) using low resolution (100 km) with identical vertical resolutions using OpenIFS (version 43r3). We find that both OpenIFS simulations and reanalysis underestimate the rates of extreme precipitation compared to observations. The biases are largest for the lowest resolution (100 km) and decrease with [higher](#) horizontal resolution (50 and 25 km) simulations in all seasons. The sensitivity to horizontal resolution is particularly high in mountain regions (such as the Alps, Scandinavia, Iberian Peninsula), likely linked to the sensitivity of vertical velocity to the representation of topography. The sensitivity of precipitation to model resolution increases dramatically with increasing percentiles, with modest biases in the 70th–80th percentile range and large biases above the 99th percentile range. We also find that precipitation above the 99th percentile mostly consists of large-scale precipitation (~80 %) in winter, while in summer it is mostly large-scale precipitation in Northern Europe (~70 %) and convective precipitation in Southern Europe (~70 %). Convective precipitation is more sensitive to model time step than to horizontal resolution. Large-scale precipitation increases significantly with both [higher](#) horizontal resolution and [shorter](#) model time step.

Deleted: increasing

Deleted: increasing

Deleted: reducing

1. Introduction

Extreme precipitation events have severe impacts on our society and ecosystems. For example, extreme precipitation caused a devastating flood in Germany in 2021, in which around 180 people died. The frequency and intensity of extreme precipitation are projected to increase over most regions in the future (Intergovernmental Panel on Climate Change, 2023; Li et al., 2021; Myhre et al., 2019). The increasing extreme precipitation poses a threat to society and must thus be realistically simulated and projected accurately for future climates. However, the climate models have large biases in simulating extreme precipitation events due to coarse horizontal resolution grid and long model time step etc. (Alexander et al., 2019; Avila et al., 2015; Sillmann et al., 2013). The model biases are also hard to evaluate as we lack long-term observations. This study aims to understand the sensitivity of extreme precipitation to model horizontal resolution and model time step.

Extreme precipitation events are usually underestimated in CMIP models (O’Gorman, 2015; Sillmann et al., 2013). Some studies found the simulated extreme precipitation at higher atmosphere horizontal resolutions is more realistic (Wehner et al., 2010, 2014). Jong et al. (2023) found that the characteristics of extreme precipitation at 25 km resolution configurations have smaller biases than at 50 and 100 km. While, Kopparla et al. (2013) found that the reduced extreme precipitation biases at higher horizontal resolution do not hold for all regions (e.g., Australia).

Strandberg and Lind (2021) reported the effect of horizontal resolution on European extreme precipitation is largest in regions with complex topography and in the summer season when precipitation is mostly caused by convective processes using coupled models, in agreement with Iles et al. (2020). However, Li et al. (2011) demonstrated that the impact of horizontal resolution on global precipitation extremes is manifested mostly by its effects on large-scale precipitation, which could be due to the improved large-scale circulation (Hack et al., 2006). Other studies also found an increasing large-scale precipitation with higher resolution but the convective precipitation is rather insensitive to resolution (Bacmeister et al., 2014; Jung et al., 2012; Kopparla et al., 2013).

70 Both the individual physical parameterization in models and their coupling to the dynamics
71 can benefit from a shorter time step (Jung et al., 2012). Mishra and Sahany (2011) found a
72 more realistic simulation of the heavy precipitation in the tropics when the time step was
73 shortened from 60 to 5 minutes at a coarse (~300 km) resolution in a short-period (12 months)
74 configuration. Jung et al. (2012) also reported that the biases in tropical circulation are smaller
75 at 15 minutes than 60 minutes in the IFS model, which is related to tropical precipitation
76 although they did not work on the precipitation in their study. However, Roberts et al. (2018)
77 found a minimal impact on model biases when shortening the time step from 20 to 15 minutes
78 at 25 km in the IFS model. They either did not investigate the multi-year precipitation extremes,
79 or did not explore the extremes in IFS model.

80 The sensitivity of climate model performance to horizontal resolution and model time step
81 exists in many models, but the level of sensitivity varies considerably between models and
82 studied regions. Most of the global atmosphere-models do not explicitly resolve all the physical
83 processes and must therefore employ parametrizations to represent those unresolved processes
84 (spatially or temporally), which shows a weakness in the models. A recent study by Savita et
85 al. (2024) explored the sensitivity of global mean precipitation to the horizontal resolution and
86 model time step in atmosphere-only simulations with OpenIFS. However, the extreme
87 precipitation's sensitivity to horizontal resolution and time step was not investigated. In this
88 study, we investigated the impact of horizontal resolutions (~100 km, ~50 km, and ~25 km)
89 and model time steps (60 minutes, 30 minutes, and 15 minutes) on daily extreme precipitation
90 using OpenIFS simulations and compare them with observation. We also studied the
91 convective and large-scale precipitation in all simulations. Precipitation extremes sensitivity to
92 model time step is the first time explored in this work using 100 km in OpenIFS atmosphere
93 model. Besides the extremes, we also explored multi-percentile precipitation's sensitivity to
94 horizontal resolution and time step. This paper is structured as follows: section 2 describes the
95 data and methodology, and section 3 discusses the results. The conclusion and discussion can
96 be found in section 4.

97
98
99
100
101
102

103 **2. Data and Methods**

104 **2.1 Model, observation, and reanalysis data**

106
107 The OpenIFS is derived from the Integrated Forecasting System at the European Centre for
108 Medium-range Weather Forecasting (ECMWF-IFS) cycle 43 release 3 (43r3) (ECMWF, 2017).
109 We use the same AMIP simulations that were used in Savita et al. (2024) which cover the
110 period 1979-2014 and are extended to 2019 using sea-surface temperature (SST) from ERA5
111 and the Shared Socioeconomic Pathway 5 (SSP5-8.5) scenario from CMIP6. OpenIFS
112 simulations use 91 vertical levels (L91) and the different horizontal resolutions: low resolution
113 (Tco95, ~100 km), medium resolution (Tco199, ~50 km), and high resolution (Tco399, ~25
114 km). For the low resolution, additional sensitivity experiments use different model time steps
115 i.e., 60, 30, and 15 minutes and we refer to these experiments as LR60m, LR30m, and LR,
116 respectively. For medium and high resolution, the same model time step is used (i.e., 15
117 minutes), of which experiments refer to as MR and HR, respectively. While the OpenIFS uses
118 a reduced octahedral grid (Malardel et al., 2016), the final output used in this study has been
119 interpolated to a regular grid using the second-order conservative method (Kritsikis et al., 2017)
120 by XIOS output server. The LR, LR30m and LR60m output were interpolated to a global 0.9°
121 regular grid while the MR and HR output were interpolated to a global 0.45° regular grid, i.e.,
122 we are not investigating extreme precipitation in high resolution simulations in their native
123 reduced octahedral grid, which will be investigated in future study. The simulations used here
124 were used by Savita et al. (2024) who found improvements in the surface zonal wind, Rossby
125 wave amplitude and phase speed, weather regime patterns, and surface-air temperature when
126 [shortening](#) a model time step from 60 minutes to 30 and 15 minutes in low resolution or
127 increasing the horizontal resolution from 100 km to 50 and 25 km. However, Savita et al. (2024)
128 did not find such improvement in the mean precipitation bias by increasing horizontal
129 resolution or [shortening](#) the model time step.

Deleted: reducing

Deleted: reducing

130 To validate OpenIFS simulations, we use the gridded daily precipitation observational data
131 from Global Precipitation Climatology Centre (GPCC) with resolution of $1^\circ \times 1^\circ$ for the period
132 1982–2019 (Ziese et al., 2022) as well as the reanalysis data from the ECMWF Reanalysis v5
133 (ERA5) for 1979–2019 (Hersbach et al., 2023). ERA5 is based on the IFS Cy41r2, with 31 km
134 horizontal resolution and 137 levels (Hersbach et al., 2020). We analyzed total, large-scale,
135 and convective precipitation in this study. The total precipitation (convective plus large-scale

precipitation) in the IFS is the accumulated precipitation, comprising of rain and snow, that falls to the Earth's surface, and it is not assimilated in the IFS. The convective precipitation is generated by the convection scheme in the IFS, which represents convection at spatial scales smaller than the grid box. The convection scheme follows Sundqvist (1978), which is also used in the OpenIFS. The large-scale precipitation is generated by the cloud scheme (Khairoutdinov and Kogan, 2000), which represents the formation and dissipation of clouds and large-scale precipitation due to changes in atmospheric quantities (such as pressure, temperature, and moisture) predicted directly by the IFS at spatial scales of the grid box or larger. The autoconversion/accretion parameterization is a non-linear function of the mass of both liquid cloud and rainwater. The calculation follows Khairoutdinov and Kogan (2000) which is derived from large eddy simulation studies of drizzling stratocumulus clouds, and this scheme is also used in OpenIFS. Several studies have evaluated the performance of ERA5 and found that the total precipitation in ERA5 is performing well over the US (Tarek et al., 2020; Xu et al., 2019). For global precipitation, the mean absolute difference over 50° S–50° N between ERA5 and TRMM/3B43 is 0.58 mm/d; the global-mean correlation with GPCP data is 0.77, which is better compared to ERA-Interim (0.63 mm/d and 0.67) (Hersbach et al., 2020). ERA5 also performs well in polar regions in representing wind, temperature and humidity (Graham et al., 2019; Tetzner et al., 2019; Wang et al., 2019).

Here we analyze daily ERA5 and the OpenIFS data over Europe (30° N–72° N, 10° W–40° E) for the period of 1982–2019 to be consistent with the GPCC dataset. For comparison, the ERA5, GPCC, MR, and HR data are remapped to LR ($\sim 0.9375^\circ \times 0.9375^\circ$) using the second-order conservative remapping method, which is consistent with the XIOS server used. The second-order conservative method includes the gradient across the source cell, which is not included in the first-order conservative method. Therefore, it gives a smoother, more accurate representation of the source field (Jones, 1998).

2.2 Methods

Calculation of q^{th} percentile value

We calculated different percentile values using total precipitation from GPCC, ERA5, and OpenIFS simulations. When we calculated the q^{th} percentile value, the normalized ranking usually did not match the location of the q^{th} percentile exactly, which means the q^{th} lies between two indices. Therefore, we determined the location first, then computed the q^{th} value by

170 interpolating between the two nearest values based on the location. Here we used the formula
171 below to find the location:

$$172 \quad j = q * (n - 1) \quad (1)$$

173 n is the length of the sample, q is the desired percentile, j is the location which is the distance
174 from the first value X_1 (X_m are the sorted sample values, $m=1, 2, \dots, n$). Then we took i as the
175 nearest (lower) integer of j to get the q^{th} value $P(q)$ by interpolating.

$$176 \quad P(q) = X_i + (X_{i+1} - X_i) * (j - i) \quad (2)$$

177 There are other methods to determine the location of q^{th} percentile (Hyndman and Fan, 1996),
178 but here we use the 'linear' one.

179

180 **The large-scale precipitation contribution to extreme precipitation**

181 To calculate the contribution of large-scale precipitation to total precipitation for a percentile
182 range, at each grid point we accumulated the large-scale precipitation on all days when the total
183 precipitation is in that percentile range, then divided it by the accumulated total precipitation
184 on those days to get the fraction of large-scale precipitation.

185

186 **Calculation of RMSE values**

187 We used the root-mean-square error (RMSE) referenced to GPCC that measures the
188 performance of ERA5 and OpenIFS simulations:

$$189 \quad \text{RMSE} = \sqrt{\frac{\sum_{i=1}^n (x_{mi} - x_{oi})^2}{n}} \quad (3)$$

190 x_{mi} is the value at i grid point for ERA5 or OpenIFS simulations, x_{oi} is the value for GPCC, n
191 is the number of land grid points over Europe. Using equation (3), we calculated the RMSE
192 values for different percentile ranges. Smaller RMSE values mean the biases between OpenIFS
193 (or ERA5) and GPCC are smaller i.e., the model simulations and ERA5 are performing better.
194 [The relative RMSE \(RRMSE\) is calculated by dividing the RMSE by GPCC precipitation at](#)
195 [corresponding percentile range.](#)

196

197 **Confidence intervals**

198 We calculated the 2.5 to 97.5th confidence intervals (CI) for the RMSE for each percentile with
199 a bootstrap method. For example, to calculate the CI for the RMSE of HR (referenced to GPCC
200 observation), we randomly chose n grid cell pairs from GPCC and HR over European land,
201 then calculated their RMSE (n is the number of total land grid points over Europe). This process
202 was repeated for 2000 times. We took the 2.5th and 97.5th percentiles of the distribution of the

203 2000 RMSEs as the 95 % CI. If the CI for different simulations do not overlap then we refer
204 that they are significantly different.

205

206 3. Results

207

208 3.1 Extreme precipitation over Europe

209

210 We show the time series of 99th percentile precipitation calculated from all grid points and all
211 days in each year over the period 1982–2019 from GPCC, ERA5, and OpenIFS simulations

212 over Europe (Fig. 1). The ERA5 simulates an inter-annual variability of the 99th percentile
213 precipitation similar to that in GPCC. For example, the peak in 2010 and the low in 1994 are

214 well reproduced in the ERA5. [ERA5 is a reanalysis product that assimilates observation of
215 precipitation, therefore, we expect it to do a better job of reproducing dry \(1994\) and wet \(2010\)](#)

216 [years than OpenIFS simulations that](#) do not reproduce the same inter-annual variability as in
217 GPCC or ERA5. [However,](#) LR and HR do reproduce the 95 % significant positive trend

218 observed in GPCC (0.03 mm/d/y, not shown), which are ~0.02 mm/d/y for both LR and HR,
219 and it is not significant for MR. We note that the OpenIFS simulations use observed SST and

220 sea-ice concentrations as boundary conditions, but ozone is taken from a photochemical
221 equilibrium (Cariolle and Teyssède, 2007) and aerosol concentrations are taken from

222 Copernicus Atmosphere Monitoring Service (CAMS) monthly climatology. Therefore, we do
223 not expect LR, MR and HR to reproduce trends driven by ozone or aerosols forcing. We also

224 find that both ERA5 and OpenIFS simulations have relatively lower 99th percentile
225 precipitation rates compared to GPCC (Fig. 1). The RMSE for ERA5 (0.36 mm/d) is lower

226 than for OpenIFS simulations which is largest for LR (2.03 mm/d) and decreases with [higher](#)
227 horizontal resolution (i.e., 1.13 mm/d for MR and 0.69 mm/d for HR). Note that Fig. 1 does

228 not contain any spatial information and that a mismatch between model data and observations
229 can be due to the 99th percentile occurring in different regions and/or with different magnitudes.

230 The RMSE analysis suggests that ERA5 and HR are close to GPCC and LR is far from GPCC.

231

232 Figure 2a–e shows the spatial distribution of the 99th percentile precipitation over Europe for
233 all days in each season for all years in GPCC, ERA5, and OpenIFS simulations, respectively.

234 In general, the extreme precipitation is very low (~ 2 mm/d) in Northern Africa, which is to be
235 expected since the mean precipitation is only 0.5 mm/d in those regions (Fig. S1). The extreme

236 precipitation exceeds 30 mm/d over mountain areas (e.g., Scandinavian mountains, Alps, and
237 Iberian Peninsula) and the north coast of the Mediterranean but is otherwise lower (~15 mm/d).

Deleted: OpenIFS simulations

Deleted: but

Deleted: increasing

241 The spatial distribution of extreme precipitation matches that of the mean precipitation pattern
 242 (Fig. S1). The high 99th percentile precipitation near mountains is likely due to the forced ascent
 243 of westerly (Scandinavia, Iberian Peninsula, British Isles) and southerly (Alps) winds. The high
 244 99th [percentile](#) precipitation in the north of the Mediterranean is likely because of warm and
 245 moist southerly winds from the Mediterranean Sea. The ERA5 and OpenIFS simulations
 246 overall reproduce the spatial distribution of the 99th percentile precipitation from GPCC.
 247 However, the magnitudes are different, particularly over the Scandinavian mountains, the Alps,
 248 and central Europe near 50° N (Fig. 2a–e). Figure 2f–i show the regional biases for the 99th
 249 percentile precipitation referenced to GPCC. LR mostly underestimates the 99th percentile
 250 precipitation in mountainous areas and deserts by more than 25 % (Fig. 2g) and the biases are
 251 reduced when horizontal resolution is increased in MR and HR (Fig. 2h–i). We also notice that
 252 LR underestimates the 99th percentile precipitation south of the Alps but overestimates it to the
 253 north (Fig. 2 (g)), whereas this bias is negligible in higher-resolution simulations (Fig. 2h–i).
 254 This [is due to the lower and gentler Alps region simulated in LR \(Fig. S2\), where](#) the moist
 255 southerly winds do not ascend high enough, therefore there is less precipitation formed on the
 256 southern side and more moisture is advected over the mountain. [The moist air descends more](#)
 257 [slowly over gentler leeward side in LR than MR \(HR\), thus the leeward region may get more](#)
 258 [precipitation.](#) The reduced biases near mountain regions in the higher-resolution simulations
 259 are likely because higher resolution has a better representation of topography and vertical
 260 velocity. A cross section of the topography and annual-mean vertical velocity at 850 hPa and
 261 62° N (Fig. [S3a&b](#)) highlight that the higher-resolution simulations resolve steeper topography,
 262 which leads to more ascent and thus more precipitation.

Deleted: could be because

Deleted: with LR

Deleted: S2 and

264 The 99th percentile precipitation over the Alps is more realistic with higher horizontal
 265 resolution compared to lower resolution. However, all simulations as well as ERA5 exhibit a
 266 negative bias over northeast Italy and west Slovenia (Fig. 2f–i). By analyzing the EOBS data,
 267 we find a similar negative bias as in GPCC, but a positive bias in GPCP (Fig. S4d–k). We notice
 268 that the extreme precipitation over the Alps (including Slovenia) in GPCP is lower than GPCC
 269 and EOBS (Fig. S4a–c), which is likely due to the different data sources and grid methods in
 270 different observation datasets (e.g., GPCC and EOBS are gauge-based gridded data on the land,
 271 but GPCP data combines microwave and infrared measurements, satellites and rain gauges).
 272 We do not know which observation dataset is more realistic, therefore, the cause of the negative
 273 bias near Slovenia could be a bias in GPCC or a persistent model bias in the ECMWF-IFS on

277 which both ERA5 and OpenIFS are based. In general, ERA5 has a lower RMSE (2.6 mm/d)
278 for extreme total precipitation than OpenIFS simulations, i.e., ERA5 has overall lower biases
279 than LR (4.0 mm/d) and is similar to MR (3.0 mm/d) and HR (2.9 mm/d).

280

281 We next calculate the trend for the annual 99th percentile precipitation over Europe (Fig. 3 &
282 4) and find that the 99th percentile precipitation has a large positive trend in central Europe and
283 a negative trend to the north of the Alps in GPCC (Fig. 3a). The ERA5 reproduces the pattern
284 of the trend found in GPCC but is not significant. However, OpenIFS simulations do not have
285 consistent patterns with GPCC (Fig. 3d-f, Fig. 4d-f), with only LR30m reproducing the large
286 positive trend in central Europe (Fig. 4d). Overall, the trend is largely underestimated over
287 central Europe but overestimated over northern Europe in OpenIFS simulations. We have not
288 found any consistent improvement across the horizontal resolution and model time step.

289

290 In addition to the 99th percentile precipitation and the trend, we calculate annual total
291 precipitation in different percentile ranges, such as 70th-80th, 80th-90th, 90th-95th, 95th-99th,
292 99th-99.5th, 99.5th-99.9th and larger than 99.9th (i.e., >99.9th) percentile. The RMSEs for ERA5
293 and OpenIFS simulations referenced to GPCC in each range are shown in Fig. 5. The RMSEs
294 increase exponentially with increasing percentiles, from less than 1 mm/d at the 70th-80th
295 percentile range to ~8 mm/d above the 99.9th percentile range. The largest RMSE is found for
296 LR60m above the 99.9th percentile range which is around 12 mm/d [CI: 11.3-12.8 mm/d]. We
297 also find that the RMSEs decrease with finer horizontal resolution for all percentile ranges. The
298 CI of the RMSEs from LR do not overlap with those from higher horizontal resolutions for any
299 percentile range, i.e., the biases from LR are significantly different from that at higher
300 resolutions and thus clearly sensitive to the horizontal resolution. Notably, the RMSE
301 differences between LR simulation and the higher-resolution simulations as well as ERA5 are
302 larger at higher percentile ranges (>95th) than those at lower percentile ranges (<95th). This
303 suggests that the extreme precipitation is more sensitive to horizontal resolution than
304 precipitation at lower percentile ranges (<95th). ERA5 has the smallest RMSE of all datasets
305 above the 95th percentile ranges, i.e., ERA5 has a better representation of the extreme
306 precipitation than our OpenIFS simulations (Fig. 5).

307

308 The RMSEs for LR60m, LR30m, and LR are smaller when the model time step is shorter.
309 However, the CI of RMSE overlaps at all percentile ranges, i.e., the sensitivity of precipitation

Deleted: c

Deleted: c

Deleted: c

Deleted: c

Deleted: c

Deleted: increasing with increasing model time steps.

316 to the model time step is not statistically significant in the low-resolution configurations. While
317 the model time step may influence precipitation, especially convective precipitation, errors
318 from poorly resolved topography probably have a large impact on the RMSE, which would
319 explain the lack of sensitivity to the model time step.

320
321 The above analysis is based on the RMSE values, which measure the absolute magnitude of
322 biases. The exponential increase in RMSE with higher percentiles is due to the corresponding
323 exponential increase in precipitation amounts across those percentiles. The relative biases are
324 further explored by calculating the relative RMSE (RRMSE) (Fig. S5). For the precipitation
325 above 90th percentile (> 6 mm/d), RRMSEs are larger at higher percentiles (>99.9th percentile)
326 than lower percentiles (90-95th percentile). A larger sensitivity to horizontal resolution at
327 higher percentiles can be also seen, since the RRMSE differences between LR and MR (HR)
328 slightly increase from 5.5% at 90-95th to 6.9% above 99.9th percentile. The above RRMSEs'
329 results are qualitatively consistent with the larger RMSE and sensitivity to horizontal resolution
330 at higher percentiles shown in Fig. 5, but quantitatively RRMSE shows smaller variations
331 across percentiles than RMSE does. However, the RRMSE at 70-90th percentile ranges show
332 comparable magnitude and sensitivity to those above 99th percentile, which is related to the
333 very low precipitation amounts at these percentiles (1.9 mm/d for 70-80th and 3.6 mm/d for 80-
334 90th percentile range).

336 3.2 Relative roles of convective and large-scale precipitation

337
338 Total precipitation is the sum of convective and large-scale precipitation. Convective
339 precipitation is related to unresolved convective motions. It comes from the physical processes
340 whose scales are smaller than the resolution of the model, therefore need to be parametrized.
341 On the other hand, large-scale precipitation is related to large-scale processes larger than the
342 model resolution, that can be resolved. When moving to higher horizontal resolutions, large-
343 scale precipitation is likely to increase, and the ratio between convective and large-scale
344 precipitation may change. In this section we split the extreme precipitation into convective and
345 large-scale precipitation to see their sensitivities to horizontal resolution and model time step.
346 The extreme precipitation is nearly 100 % large-scale precipitation over northern Europe, more
347 than 90 % over central Europe, and more than 70 % over western and southern Europe in DJF
348 (Fig. 6e-h). However, in JJA the extreme precipitation is mostly large-scale precipitation over
349 northern Europe (>70 %) and convective precipitation in the Mediterranean region (>70 %)

Deleted: unsolved

Deleted: As the horizontal resolution become higher

Deleted: consist of

353 (Fig. 6a–d). Due to the seasonal dependent large-scale precipitation contribution to extreme
354 total precipitation, we discuss convective and large-scale precipitation’s sensitivities to
355 horizontal resolution and time step in JJA and DJF separately. The ratios between convective
356 and large-scale precipitation are also discussed here. Considering the ratios over [parts of](#)
357 [Mediterranean](#) region are very large, which influence the results a lot, we remove [that region](#)
358 and only include the region north than 40°N (i.e., 40° N–72° N, 10° W–40° E) in this section.

Deleted: north African

Deleted: north Africa

359 During the extreme precipitation days, Europe has more convective precipitation in JJA (~10
360 mm/d) than in DJF (~3.7 mm/d), and their distributions do not change much across horizontal
361 resolution (Fig. 7a & b). While, from the significant test (Table 2a), we found JJA convective
362 precipitation only increases significantly moving from MR to HR, and DJF convective
363 precipitation significantly increases from LR to MR (HR). However, convective precipitation’s
364 distributions vary noticeably across model time steps, as shown in Fig. 7 c & d. As the model
365 time step reduces, the distributions of JJA convective precipitation move to the left, thus less
366 convective precipitation are simulated in shorter time step simulations. DJF has similar results
367 as in JJA. The changes are significant (Table 2a), that is, convective precipitation in OpenIFS
368 is sensitive to model time step.

370 The distributions of large-scale precipitation in MR and HR (Fig. 7e) shift to the right compared
371 to LR in JJA, and MR and HR have significantly more large-scale precipitation (13.2 mm/d)
372 than LR (11.4 mm/d). In DJF, the distribution peak of LR, MR and HR are similar (Fig. 7f),
373 but MR and HR have bigger tails than LR. Thus, MR and HR have more large-scale
374 precipitation than LR. The increase of large-scale precipitation is likely due to the better
375 simulated topography at higher horizontal resolution, where more large-scale precipitation is
376 resolved. The changes of large-scale precipitation in both JJA and DJF from LR to MR are
377 significant, but not from MR to HR (Table 2b). That means, the large-scale precipitation is
378 sensitive when horizontal resolution is increased from LR to MR, but not from MR to HR.
379 Large-scale precipitation also significantly increases when the model time step is shorten from
380 60 min to 30 min, and also from 30 min to 15 min in both JJA (Fig. 7g) and DJF (Fig. 7h), that
381 is large-scale precipitation is also sensitive to the model time step.

383 We further analyse the distribution of ratio between convective and large-scale precipitation in
384 JJA and DJF, shown in Fig. 8. For different resolutions, the ratio distributions from MR and
385 HR are narrower and slightly shift to the left compared to LR in JJA (Fig. 8a), which means
386

MR and HR have smaller mean ratios (1.5) than LR (~1.25). That is due to the large-scale precipitation increasing by 16% with finer horizontal resolution, whereas convective precipitation only increases by 6%. However, the ratio between convective and large-scale precipitation do not vary significantly with higher horizontal resolutions in DJF (Fig. 8b). When moving to shorter model time step, the ratios significantly decrease in JJA (from 2 to 1.5) and DJF (Fig. 8c-d, Table 2c). It is related to the significant decreasing convective and increasing large-scale precipitation with shorter model time step.

In summary, during extreme precipitation days, large-scale precipitation increases with higher horizontal resolution and shorter model time step, however, convective precipitation increases with higher horizontal resolution and decrease with shorter model time step. Convective precipitation is more sensitive to model time steps than to horizontal resolutions, while large-scale precipitation is sensitive to both. Therefore, the extreme precipitation sensitivity to horizontal resolution is mostly from large-scale precipitation.

We also analyse the mean state convective and large-scale precipitation's sensitivity to horizontal resolution and model time step (Fig. S6 & S7). Convective precipitation decreases and large-scale precipitation increases with higher horizontal resolution and shorter model time step, therefore their ratio decreases. Their sensitivities to resolutions and time steps are less significant in mean state than in extreme state, especially for mean convective precipitation, which is only significantly sensitive when shortening model time step from 30 min to 15 min. The changes of mean convective precipitation with horizontal resolution are opposite with the extreme one (Fig. S6a & b, Fig. 7a & b), but these changes for both extreme and mean states are very little, and convective precipitation is more sensitive to model time steps in both states (Fig. S6c & d, Fig. 7c & d).

4. Discussion and Conclusion

We have investigated the sensitivity of extreme precipitation across different horizontal resolutions and model time steps in atmosphere-only experiments with the OpenIFS. Comparing extreme precipitation (defined as total daily precipitation at the 99th percentile) from OpenIFS simulations, reanalysis (ERA5), and observation (GPCC), we find that MR and HR mostly better represent the precipitation extremes compared to LR. We also found a more significant sensitivity to the horizontal resolution for the precipitation above the 95th percentile and less sensitivity for lower percentile ranges (<95th) (Fig. 5). These OpenIFS-based results

Deleted: It is likely due to that large-scale precipitation increase by a larger percentage with increasing resolution than convective precipitation.

Deleted:

Deleted: changing

Deleted: It is likely due to that both large-scale and convective precipitation increase in similar magnitude with increasing horizontal resolution, therefore, the ratio's changes with resolutions are not always significant.

Deleted: we reduce the

Deleted: the distributions of ratios in JJA shift to the left (from 2 to 1.5), which means the ratio decreases with the reducing time step (Fig. 8c). In

Deleted: the peaks of ratio of LR60m, LR30m and LR occur in the similar position (Fig. 8d), but more values fall near the peaks in shorter time step simulations, therefore, ratio decreases when time step is reduced in DJF as well. The ratio decreases significantly as time step reduces in both JJA and DJF (Table 2c).

Deleted: i

Deleted: reducing

Deleted: when horizontal resolution increases, convective and large-scale precipitation will increase, while their ratio will decrease. When model time step reduces, convective precipitation will decrease, large-scale precipitation will increase, therefore their ratio will decrease.

Deleted: With increasing horizontal resolution and reducing model time step,

Deleted: c

Deleted: ,

Deleted: and

Deleted: reducing

Deleted: Additionally, we analyse the precipitation on their native resolution to see the impact of coarsening the horizontal resolution. The native resolution of our model output is 192×384 for LR, 400×800 for MR and HR. Due to the computational expense and time, we only saved a coarser resolution for HR, but not on the original resolution (i.e., ~800×1600). Similar to the result of coarsened data (Fig. 1), extreme precipitation on their native resolution is underestimated in OpenIFS compared to GPCC, and the biases decrease with increasing horizontal resolution (Fig. 9). Extreme precipitation on native resolutions also has similar spatial distribution with that on coarsened resolution (Fig. 10, Fig. 2), such as more extreme precipitation in mountain areas. However, the extreme precipitation is larger (13% for GPCC, 7% for MR and 12% HR) on native resolution than on coarsened resolution, because some extreme precipitation is smoothed during coarsening to 0.9 × 0.9 degree.

Convective and large-scale precipitation during extreme precipitation days increase with increasing horizontal resolution (Fig. 11 a-d) and consistent with coarsened resolution results. The ratio between convective and large-scale precipitation on native resolution significantly decreases from LR to MR in JJA (Fig. 11e), which is also consistent with coarsened resolution. However, the ratio increases from MR to HR in JJA on native resolution, which is not con...

are similar to Kopparla et al. (2013), who found that the bias of extreme precipitation in the high-resolution simulation (25 km) is reduced compared to the lower-resolution simulations (100 km and 200 km) over Europe in their atmospheric model, but not for precipitation at lower percentiles (i.e., <95th). However, the sensitivity to the horizontal resolution found by Kopparla et al. (2013) was not significant over Europe which is rather different from our results as we have found a significant difference across the horizontal resolutions. In contrast to the extreme precipitation, the bias for global mean precipitation is not decreasing much with [higher](#) horizontal resolution in OpenIFS. Similar results are also found in other AGCMs (e.g., ECHAM6, OpenIFS, HadGEM1 and HadGEM3) (Hertwig et al., 2015; Savita et al., 2024; Schiemann et al., 2014; Demory et al., 2020;). However, Delworth et al. (2012) found an improvement in the global mean precipitation with [higher](#) horizontal resolution in a coupled model (GFDL).

Deleted: increasing

Deleted: increasing

The improvements due to [higher](#) horizontal resolution for the extreme precipitation are mostly over the mountain areas, consistent with previous studies which found the effect of horizontal resolution being largest in areas with complex topography over Europe and also other regions for mean and extreme precipitation (Demory et al., 2020; Iles et al., 2020; Monerie et al., 2020; Prein et al., 2013; Torma et al., 2015). The sensitivity to the horizontal resolution comes from the large-scale precipitation, which is likely because of the better-resolved topography. However, the convective precipitation is more sensitive to the model time step than it is to the horizontal resolution.

Deleted: increasing

In our results, larger improvements are obtained when the horizontal resolution is increased from LR to MR, but relatively smaller improvements from MR to HR. This diminishing return is also found by Roberts et al. (2018) from ~50 km to ~25 km in ECMWF-IFS, but for climatological surface biases. The simulation of extratropical cyclones, tropospheric circulation and tropical mean precipitation in ECMWF-IFS also have smaller improvements from 39 km to 16 km than that from 126 km to 39 km (Jung et al., 2012). However, the tropical cyclone intensity and intense storm structure, which often cause extreme precipitation in tropics (Gori et al., 2022; Zhu and Quiring, 2022) are adequately simulated at 16 km, but not at 126 and 39 km resolutions in ECMWF-IFS (Manganello et al., 2012). Therefore, the diminishing return in this study is valid for European extreme precipitation, but may not for tropical extreme precipitation.

Since the analysis of horizontal resolution's impact is based on regridded data, may therefore be influenced by the regridding process. The native resolution of our model output is 192×384 for LR, 400×800 for MR and 800×1600 for HR, however, only 400×800 for HR output is saved due to computational cost. Similar to the result of regridded data (Fig. 1), extreme precipitation on their native resolution is underestimated in OpenIFS compared to GPCC, and the biases decrease with higher horizontal resolution (Fig. 9). Extreme precipitation on native resolutions also has similar spatial distribution with that on regridded resolution (Fig. 10, Fig. 2), such as more extreme precipitation in mountain areas. However, the extreme precipitation is larger (13% for GPCC, 7% for MR and 12% HR) on native resolution than on regridded resolution, because some extreme precipitation is smoothed when regridding to 0.9×0.9 degree. The RMSEs of extreme precipitation against GPCC are also larger on native resolution (Fig. 9) than on regridded resolution (Fig. 1), which holds across different percentiles (Fig. S8). Moreover, the sensitivity of extreme precipitation to horizontal resolution is also greater on native resolution (Fig. S8). Convective and large-scale precipitation during extreme precipitation days increase with higher horizontal resolution (Fig. 11 a-d), consistent with regridded results. The convective-to-large-scale precipitation ratio significantly decreases from LR to MR in JJA (Fig. 11e), which is also consistent with regridded results. However, the ratio increases from MR to HR in JJA on native resolution, differing from regridded analysis, likely due to the dramatic increasing convective precipitation from MR to HR in JJA. Overall, regridding the model dataset does not change the conclusion qualitatively in this study but causes quantitative differences.

Moreover, the choice of observation dataset is a key factor for assessing the impact of the horizontal resolution and model time step on extreme precipitation. Most observation precipitation data are from one of the three categories, gauge-based products, satellite products, and merged satellite-gauge products. Since the satellite products are constructed with satellite microwave and/ or infrared measurements, with/ without gauged-adjusted estimates, differences exist between these products. Besides, the gauge-based products are highly dependent on the choice of stations and interpolation schemes. It is hard to say which product is closer to reality, as different regions may have different observation datasets that suit best for the analysis. In particular, we note that not all products are suitable for extreme analysis. For example, GPCP's main scope is to construct a reliable climate data record and has been developed with a priority of ensuring the long-term stability of data (Adler et al., 2017). Masunaga et al. (2019) found that the frequency of GPCP daily precipitation quickly drops

below all other datasets once the precipitation exceeds 30 mm/d. Also, the time series of GPCP extreme precipitation over the ocean exhibits a jump to lower 99th percentiles in late 2008/early 2009 which is not present in all other datasets, coinciding with the change in utilization of SSM/I and SSMIS. The lower 99th precipitation suggests that the GPCP dataset might not be applied to extreme analysis (Masunaga et al., 2019). Therefore, we only use GPCC observation data as the reference to explore the model performance. In Fig. 2f–i the 99th percentile precipitation is largely underestimated in the eastern Alp region by ERA5 and all model simulations. The biases are insensitive to horizontal resolution. It is likely a persistent model bias in the ECMWF-IFS or a bias in GPCC. [Comparing model output to multiple observational precipitation products instead of relying on a single one may be a good way to reduce these biases. Multiple observational products can be taken as an ensemble, which provide a spread of observational estimates and allow insights into whether and which model configurations sit within this observational spread.](#)

Deleted: Analyzing

Code and data variability

The OpenIFS model requires a software license agreement with ECMWF to use it, and OpenIFS's license is easily given free of charge to any academic or research institute. The details of OpenIFS are available at <https://confluence.ecmwf.int/display/OIFS/About+OpenIFS> (ECMWF, 2018). We used the same simulation that used in Savita et al. (2024) and therefore do not provide the data needed to reproduce the simulations here. All data (runscripts, input data etc) needed to reproduce the simulations can be found in Savita et al. (2024) in code and data variability section. The jupyter notebook scripts used in this study to produce the plots can be found at <https://doi.org/10.5281/zenodo.15497274>. The raw model output is available from the authors upon reasonable request. The observation and reanalysis datasets used in this study can be downloaded from GPCC (https://opendata.dwd.de/climate_environment/GPCC/html/fulldata-daily_v2022_doi_download.html, Ziese et al., 2022) and ERA5 (<https://cds.climate.copernicus.eu/cdsapp#!/dataset/reanalysis-era5-single-levels?tab=form>, Hersbach et al., 2023).

Deleted: <https://doi.org/10.5281/zenodo.10887652>

Formatted: Font: (Default) Times New Roman, (Asian) Times New Roman, 12 pt, No underline, Font colour: Text 1, English (US), Ligatures: None

Authors contributions. AS and JK conducted all the OpenIFS simulations. YL did the analysis and writing with substantial contribution from JK, AS and WP.

619 **Competing interests.** The contact author has declared that none of the authors has any
620 competing interests.

621
622 **Acknowledgements.** Yingxue Liu is supported by China Scholarship Council (CSC, grant no.
623 202004910401). Joakim Kjellsson and Abhishek Savita are supported by JPI Climate/Ocean
624 (ROADMAP project, grant no. 01LP2002C). Wonsun Park was supported by IBS (grant no.
625 IBS-R028-D1). We thank the OpenIFS team at ECMWF for the technical support. All the
626 OpenIFS simulations were conducted on the HLRN machine under shk00018 project resources.
627 All the analysis and data storage were conducted on computer clusters at GEOMAR and Kiel
628 University Computing Center (NESH).

629
630 **Financial support.** This research is financially supported by CSC (grant no. 202004910401)
631 and ROADMAP project (grant no. 01LP2002C).

632
633
634
635
636
637
638
639
640
641
642
643
644
645
646
647
648
649
650
651

652

653 References

- 654 Adler, R. F., Gu, G., Sapiiano, M., Wang, J. J., and Huffman, G. J.: Global Precipitation:
655 Means, Variations and Trends During the Satellite Era (1979–2014),
656 <https://doi.org/10.1007/s10712-017-9416-4>, 1 July 2017.
- 657 Alexander, L. V., Fowler, H. J., Bador, M., Behrangi, A., Donat, M. G., Dunn, R., Funk,
658 C., Goldie, J., Lewis, E., Rogé, M., Seneviratne, S. I., and Venugopal, V.: On the use of
659 indices to study extreme precipitation on sub-daily and daily timescales, *Environmental*
660 *Research Letters*, 14, <https://doi.org/10.1088/1748-9326/ab51b6>, 2019.
- 661 Avila, F. B., Dong, S., Menang, K. P., Rajczak, J., Renom, M., Donat, M. G., and
662 Alexander, L. V.: Systematic investigation of gridding-related scaling effects on annual
663 statistics of daily temperature and precipitation maxima: A case study for south-east
664 Australia, *Weather Clim Extrem*, 9, 6–16, <https://doi.org/10.1016/j.wace.2015.06.003>,
665 2015.
- 666 Bacmeister, J. T., Wehner, M. F., Neale, R. B., Gettelman, A., Hannay, C., Lauritzen, P.
667 H., Caron, J. M., and Truesdale, J. E.: Exploratory high-resolution climate simulations
668 using the community atmosphere model (CAM), *J Clim*, 27, 3073–3099,
669 <https://doi.org/10.1175/JCLI-D-13-00387.1>, 2014.
- 670 Bell, B., Hersbach, H., Simmons, A., Berrisford, P., Dahlgren, P., Horányi, A., Muñoz-
671 Sabater, J., Nicolas, J., Radu, R., Schepers, D., Soci, C., Villaume, S., Bidlot, J. R.,
672 Haimberger, L., Woollen, J., Buontempo, C., and Thépaut, J. N.: The ERA5 global
673 reanalysis: Preliminary extension to 1950, *Quarterly Journal of the Royal*
674 *Meteorological Society*, 147, 4186–4227, <https://doi.org/10.1002/qj.4174>, 2021.
- 675 Cariolle, D. and Teyssède, H.: Atmospheric Chemistry and Physics A revised linear ozone
676 photochemistry parameterization for use in transport and general circulation models:
677 multi-annual simulations, *Atmos. Chem. Phys*, 2183–2196 pp., 2007.
- 678 Delworth, T. L., Rosati, A., Anderson, W., Adcroft, A. J., Balaji, V., Benson, R., Dixon,
679 K., Griffies, S. M., Lee, H. C., Pacanowski, R. C., Vecchi, G. A., Wittenberg, A. T.,
680 Zeng, F., and Zhang, R.: Simulated climate and climate change in the GFDL CM2.5
681 high-resolution coupled climate model, *J Clim*, 25, 2755–2781,
682 <https://doi.org/10.1175/JCLI-D-11-00316.1>, 2012.
- 683 Demory, M. E., Berthou, S., Fernández, J., Sørland, S. L., Brogli, R., Roberts, M. J.,
684 Beyerle, U., Seddon, J., Haarsma, R., Schär, C., Buonomo, E., Christensen, O. B.,
685 Ciarlo, J. M., Fealy, R., Nikulin, G., Peano, D., Putrasahan, D., Roberts, C. D., Senan,
686 R., Steger, C., Teichmann, C., and Vautard, R.: European daily precipitation according
687 to EURO-CORDEX regional climate models (RCMs) and high-resolution global climate
688 models (GCMs) from the High-Resolution Model Intercomparison Project
689 (HighResMIP), *Geosci Model Dev*, 13, 5485–5506, <https://doi.org/10.5194/gmd-13-5485-2020>, 2020.
- 690 ECMWF: IFS Documentation CY43R3 - Part IV: Physical processes,
691 <https://doi.org/10.21957/efyk72kl>, 2017.
- 692 Gori, A., Lin, N., Xi, D., and Emanuel, K.: Tropical cyclone climatology change greatly
693 exacerbates US extreme rainfall–surge hazard, *Nat Clim Chang*, 12, 171–178,
694 <https://doi.org/10.1038/s41558-021-01272-7>, 2022.
- 695 Graham, R. M., Hudson, S. R., and Maturilli, M.: Improved Performance of ERA5 in
696 Arctic Gateway Relative to Four Global Atmospheric Reanalyses, *Geophys Res Lett*, 46,
697 6138–6147, <https://doi.org/10.1029/2019GL082781>, 2019.

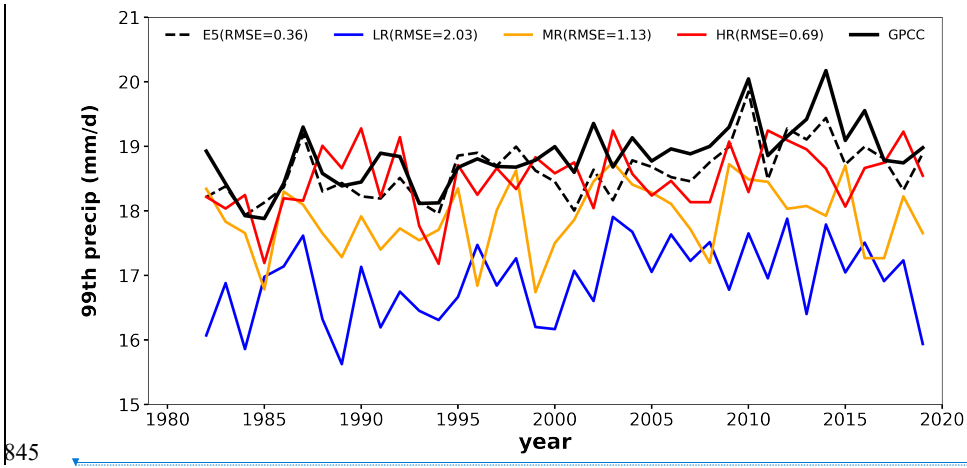
- Hack, J. J., Caron, J. M., Danabasoglu, G., Oleson, K. W., Bitz, C., and Truesdale, J. E.: CCSM-CAM3 Climate Simulation Sensitivity to Changes in Horizontal Resolution, 2006.
- Hassler, B. and Lauer, A.: Comparison of reanalysis and observational precipitation datasets including era5 and wfde5, Atmosphere (Basel), 12, <https://doi.org/10.3390/atmos12111462>, 2021.
- Hersbach, H., Bell, B., Berrisford, P., Hirahara, S., Horányi, A., Muñoz-Sabater, J., Nicolas, J., Peubey, C., Radu, R., Schepers, D., Simmons, A., Soci, C., Abdalla, S., Abellan, X., Balsamo, G., Bechtold, P., Biavati, G., Bidlot, J., Bonavita, M., De Chiara, G., Dahlgren, P., Dee, D., Diamantakis, M., Dragani, R., Flemming, J., Forbes, R., Fuentes, M., Geer, A., Haimberger, L., Healy, S., Hogan, R. J., Hólm, E., Janisková, M., Keeley, S., Laloyaux, P., Lopez, P., Lupu, C., Radnoti, G., de Rosnay, P., Rozum, I., Vamborg, F., Villaume, S., and Thépaut, J. N.: The ERA5 global reanalysis, Quarterly Journal of the Royal Meteorological Society, 146, 1999–2049, <https://doi.org/10.1002/qj.3803>, 2020.
- Hersbach, H., Bell, B., Berrisford, P., Biavati, G., Horányi, A., Muñoz Sabater, J., Nicolas, J., Peubey, C., Radu, R., Rozum, I., Schepers, D., Simmons, A., Soci, C., Dee, D., Thépaut, J.-N.: ERA5 hourly data on single levels from 1940 to present. Copernicus Climate Change Service (C3S) Climate Data Store (CDS), DOI: 10.24381/cds.adbb2d47, 2023 (Accessed on 16-09-2022).
- Hertwig, E., von Storch, J. S., Handorf, D., Dethloff, K., Fast, I., and Krismer, T.: Effect of horizontal resolution on ECHAM6-AMIP performance, Clim Dyn, 45, 185–211, <https://doi.org/10.1007/s00382-014-2396-x>, 2015.
- Hyndman, R. J. and Fan, Y.: Sample Quantiles in Statistical Packages, Source: The American Statistician, 361–365 pp., 1996.
- Iles, C. E., Vautard, R., Strachan, J., Joussaume, S., Eggen, B. R., and Hewitt, C. D.: The benefits of increasing resolution in global and regional climate simulations for European climate extremes, Geosci Model Dev, 13, 5583–5607, <https://doi.org/10.5194/gmd-13-5583-2020>, 2020.
- Intergovernmental Panel on Climate Change: Weather and Climate Extreme Events in a Changing Climate, in: Climate Change 2021 – The Physical Science Basis, Cambridge University Press, 1513–1766, <https://doi.org/10.1017/9781009157896.013>, 2023.
- Jones, P. W.: First-and Second-Order Conservative Remapping Schemes for Grids in Spherical Coordinates, 1998.
- Jong, B. T., Delworth, T. L., Cooke, W. F., Tseng, K. C., and Murakami, H.: Increases in extreme precipitation over the Northeast United States using high-resolution climate model simulations, NPJ Clim Atmos Sci, 6, <https://doi.org/10.1038/s41612-023-00347-w>, 2023.
- Jung, T., Miller, M. J., Palmer, T. N., Towers, P., Wedi, N., Achuthavarier, D., Adams, J. M., Altshuler, E. L., Cash, B. A., Kinter, J. L., Marx, L., Stan, C., and Hodges, K. I.: High-resolution global climate simulations with the ECMWF model in project athena: Experimental design, model climate, and seasonal forecast skill, J Clim, 25, 3155–3172, <https://doi.org/10.1175/JCLI-D-11-00265.1>, 2012.
- Khairoutdinov, M. and Kogan, Y.: A New Cloud Physics Parameterization in a Large-Eddy Simulation Model of Marine Stratocumulus, 2000.
- Kopparla, P., Fischer, E. M., Hannay, C., and Knutti, R.: Improved simulation of extreme precipitation in a high-resolution atmosphere model, Geophys Res Lett, 40, 5803–5808, <https://doi.org/10.1002/2013GL057866>, 2013.

- Kritsikis, E., Aechtner, M., Meurdesoif, Y., and Dubos, T.: Conservative interpolation between general spherical meshes, *Geosci Model Dev*, 10, 425–431, <https://doi.org/10.5194/gmd-10-425-2017>, 2017.
- Lavers, D. A., Simmons, A., Vamborg, F., and Rodwell, M. J.: An evaluation of ERA5 precipitation for climate monitoring, *Quarterly Journal of the Royal Meteorological Society*, 148, 3152–3165, <https://doi.org/10.1002/qj.4351>, 2022.
- Li, C., Zwiers, F., Zhang, X., Li, G., Sun, Y., and Wehner, M.: Changes in Annual Extremes of Daily Temperature and Precipitation in CMIP6 Models, *J Clim*, 34, 3441–3460, <https://doi.org/10.1175/JCLI-D-19>, 2021.
- Li, F., Collins, W. D., Wehner, M. F., Williamson, D. L., Olson, J. G., and Algieri, C.: Impact of horizontal resolution on simulation of precipitation extremes in an aqua-planet version of Community Atmospheric Model (CAM3), n.d.
- Malardel, S., Wedi, N., Deconinck, W., and Kühnlein, C.: A new grid for the IFS, 2016.
- Manganello, J. V., Hodges, K. I., Kinter, J. L., Cash, B. A., Marx, L., Jung, T., Achuthavarier, D., Adams, J. M., Altshuler, E. L., Huang, B., Jin, E. K., Stan, C., Towers, P., and Wedi, N.: Tropical cyclone climatology in a 10-km global atmospheric GCM: Toward weather-resolving climate modeling, *J Clim*, 25, 3867–3893, <https://doi.org/10.1175/JCLI-D-11-00346.1>, 2012.
- Masunaga, H., Schröder, M., Furuzawa, F. A., Kummerow, C., Rustemeier, E., and Schneider, U.: Inter-product biases in global precipitation extremes, *Environmental Research Letters*, 14, <https://doi.org/10.1088/1748-9326/ab5da9>, 2019.
- Mishra, S. K. and Sahany, S.: Effects of time step size on the simulation of tropical climate in NCAR-CAM3, *Clim Dyn*, 37, 689–704, <https://doi.org/10.1007/s00382-011-0994-4>, 2011.
- Monerie, P. A., Chevuturi, A., Cook, P., Klingaman, N. P., and Holloway, C. E.: Role of atmospheric horizontal resolution in simulating tropical and subtropical South American precipitation in HadGEM3-GC31, *Geosci Model Dev*, 13, 4749–4771, <https://doi.org/10.5194/gmd-13-4749-2020>, 2020.
- Myhre, G., Alterskjær, K., Stjern, C. W., Hodnebrog, M., Samset, B. H., Sillmann, J., Schaller, N., Fischer, E., Schulz, M., and Stohl, A.: Frequency of extreme precipitation increases extensively with event rareness under global warming, *Sci Rep*, 9, <https://doi.org/10.1038/s41598-019-52277-4>, 2019.
- O’Gorman, P. A.: Precipitation Extremes Under Climate Change, <https://doi.org/10.1007/s40641-015-0009-3>, 1 June 2015.
- Prein, A. F., Gobiet, A., Suklitsch, M., Truhetz, H., Awan, N. K., Keuler, K., and Georgievski, G.: Added value of convection permitting seasonal simulations, *Clim Dyn*, 41, 2655–2677, <https://doi.org/10.1007/s00382-013-1744-6>, 2013.
- Roberts, C. D., Senan, R., Molteni, F., Boussetta, S., Mayer, M., and Keeley, S. P. E.: Climate model configurations of the ecmwf integrated forecasting system (ecmwf-ifs cycle 43r1) for highresmp, *Geosci Model Dev*, 11, 3681–3712, <https://doi.org/10.5194/gmd-11-3681-2018>, 2018.
- Savita, A., Kjellsson, J., Kedzierski, R. P., Latif, M., Rahm, T., Wahl, S., and Park, W.: Assessment of climate biases in OpenIFS version 43r3 across model horizontal resolutions and time steps, *Geosci Model Dev*, 17, 1813–1829, <https://doi.org/10.5194/gmd-17-1813-2024>, 2024.
- Schiemann, R., Demory, M. E., Mizielinski, M. S., Roberts, M. J., Shaffrey, L. C., Strachan, J., and Vidale, P. L.: The sensitivity of the tropical circulation and Maritime Continent precipitation to climate model resolution, *Clim Dyn*, 42, 2455–2468, <https://doi.org/10.1007/s00382-013-1997-0>, 2014.

- Sillmann, J., Kharin, V. V., Zhang, X., Zwiers, F. W., and Bronaugh, D.: Climate extremes indices in the CMIP5 multimodel ensemble: Part 1. Model evaluation in the present climate, *Journal of Geophysical Research Atmospheres*, 118, 1716–1733, <https://doi.org/10.1002/jgrd.50203>, 2013.
- Strandberg, G. and Lind, P.: The importance of horizontal model resolution on simulated precipitation in Europe – from global to regional models, *Weather and Climate Dynamics*, 2, 181–204, <https://doi.org/10.5194/wcd-2-181-2021>, 2021.
- Sundqvist, H.: A parameterization scheme for non-convective condensation including prediction of cloud water content, *Quarterly Journal of the Royal Meteorological Society*, 104, 677–690, <https://doi.org/10.1002/qj.49710444110>, 1978.
- Tarek, M., Brissette, F. P., and Arsenault, R.: Evaluation of the ERA5 reanalysis as a potential reference dataset for hydrological modelling over North America, *Hydrol Earth Syst Sci*, 24, 2527–2544, <https://doi.org/10.5194/hess-24-2527-2020>, 2020.
- Tetzner, D., Thomas, E., and Allen, C.: A validation of ERA5 reanalysis data in the southern antarctic peninsula—Ellsworth land region, and its implications for ice core studies, *Geosciences (Switzerland)*, 9, <https://doi.org/10.3390/geosciences9070289>, 2019.
- Torma, C., Giorgi, F., and Coppola, E.: Added value of regional climate modeling over areas characterized by complex terrain-precipitation over the Alps, *J Geophys Res*, 120, 3957–3972, <https://doi.org/10.1002/2014JD022781>, 2015.
- Wang, C., Graham, R. M., Wang, K., Gerland, S., and Granskog, M. A.: Comparison of ERA5 and ERA-Interim near-surface air temperature, snowfall and precipitation over Arctic sea ice: effects on sea ice thermodynamics and evolution, *Cryosphere*, 13, 1661–1679, <https://doi.org/10.5194/tc-13-1661-2019>, 2019.
- Wehner, M. F., Smith, R. L., Bala, G., and Duffy, P.: The effect of horizontal resolution on simulation of very extreme US precipitation events in a global atmosphere model, *Clim Dyn*, 34, 241–247, <https://doi.org/10.1007/s00382-009-0656-y>, 2010.
- Wehner, M. F., Reed, K. A., Li, F., Prabhat, Bacmeister, J., Chen, C. T., Paciorek, C., Gleckler, P. J., Sperber, K. R., Collins, W. D., Gettelman, A., and Jablonowski, C.: The effect of horizontal resolution on simulation quality in the Community Atmospheric Model, CAM5.1, *J Adv Model Earth Syst*, 6, 980–997, <https://doi.org/10.1002/2013MS000276>, 2014.
- Xu, X., Frey, S. K., Boluwade, A., Erler, A. R., Khader, O., Lapen, D. R., and Sudicky, E.: Evaluation of variability among different precipitation products in the Northern Great Plains, *J Hydrol Reg Stud*, 24, <https://doi.org/10.1016/j.ejrh.2019.100608>, 2019.
- Zhu, L. and Quiring, S. M.: Exposure to precipitation from tropical cyclones has increased over the continental United States from 1948 to 2019, *Commun Earth Environ*, 3, <https://doi.org/10.1038/s43247-022-00639-8>, 2022.
- Ziese, Markus; Rauthe-Schöch, Armin; Becker, Andreas; Finger, Peter; Rustemeier, Elke; Hänsel, Stephanie; Schneider, Udo: GPCC Full Data Daily Version 2022 at 1.0°: Daily Land-Surface Precipitation from Rain-Gauges built on GTS-based and Historic Data. DOI: 10.5676/DWD_GPCC/FD_D_V2022_100, 2022

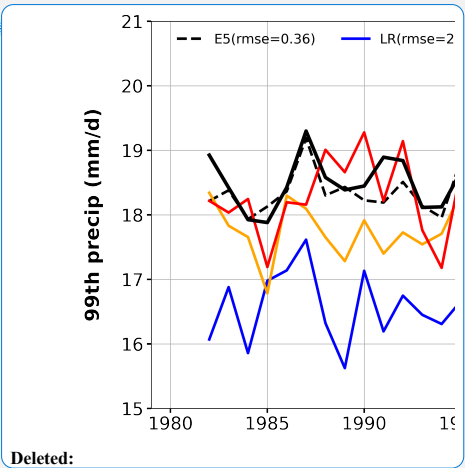
843
844

Figures

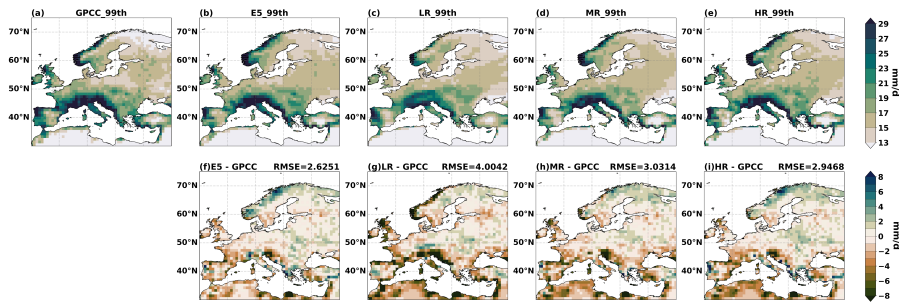


845
846
847 **Fig. 1** Annual time series of the 99th percentile precipitation using observations (GPCC, black
848 solid line), reanalysis (ERA5, black dash line), and model simulations (LR: blue, MR: orange,
849 HR: red) during 1982-2019 over Europe. RMSE values of 99th percentile precipitation are
850 computed referenced to GPCC which are shown within the small bracket ([unit: mm/d](#)).

851
852
853
854
855
856
857
858
859
860
861
862
863
864
865
866
867
868
869
870
871
872



874
875
876



877
878

879 **Fig. 2** The 99th percentile precipitation over Europe during 1982-2019 from (a) GPCC
880 observations, (b) ERA5 reanalysis, (c) LR, (d) MR, (e) HR, and the corresponding biases and
881 RMSEs in (f) ERA5, (g) LR, (h) MR, and (i) HR.

882
883
884
885
886
887
888
889
890
891
892
893
894
895
896
897
898
899
900
901
902
903
904

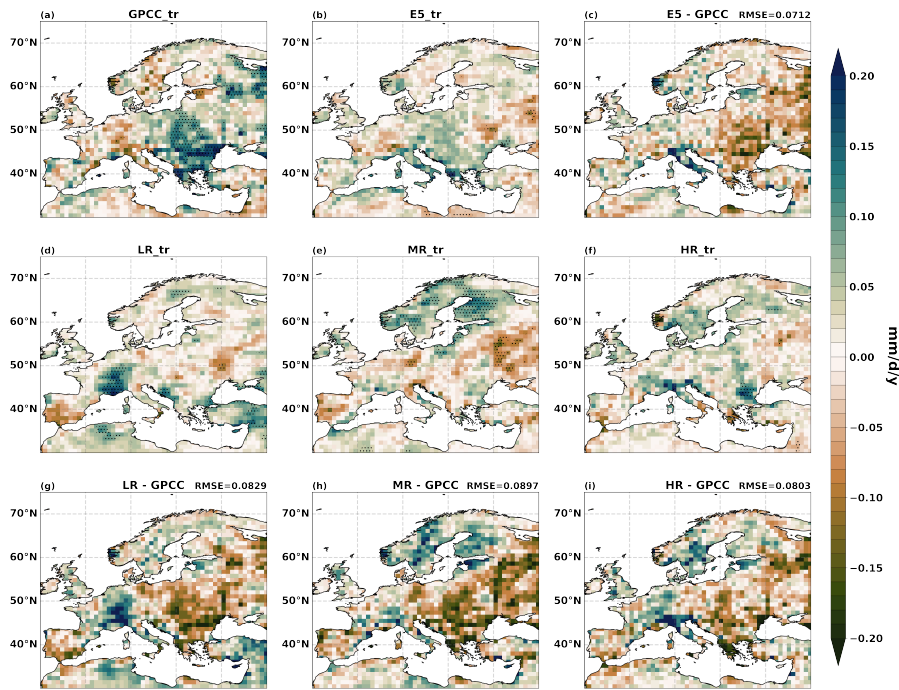
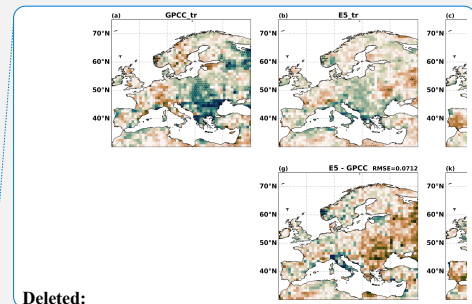


Fig. 3 The linear trends of annual 99th percentile precipitation over Europe during 1982-2019 from (a) GPCC observations, (b) ERA5 reanalysis, (d) LR, (e) MR, (f) HR, and the corresponding biases and RMSEs in (c) ERA5, (g) LR, (h) MR, (i) HR. The shadings are trends at 95 % significance levels.



Deleted:

Deleted: c

Deleted: d

Deleted: e

Deleted: f

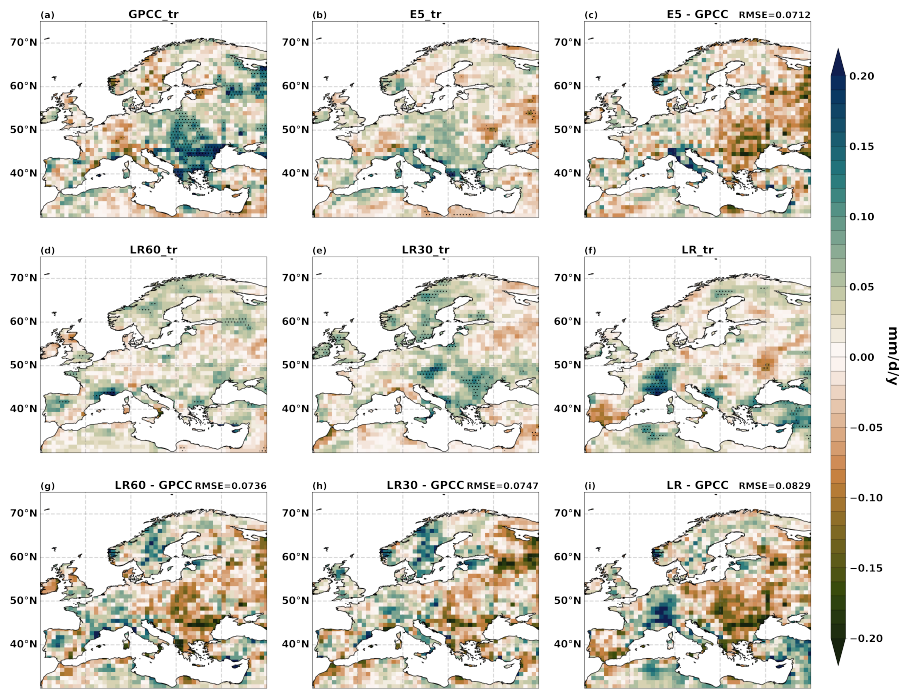
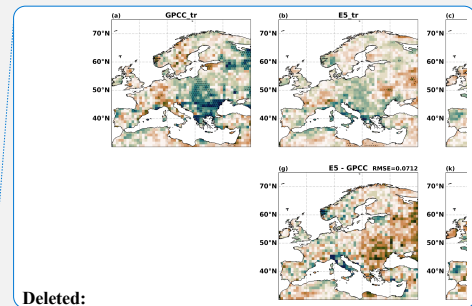


Fig. 4 The linear trends of annual 99th percentile precipitation over Europe during 1982-2019 from (a) GPCC observations, (b) ERA5 reanalysis, (d) LR60m, (e) LR30m, (f) LR, and the corresponding biases and RMSEs in (c) ERA5, (g) LR60m, (h) LR30m, (i) LR. The shadings are trends at 95 % significance levels.



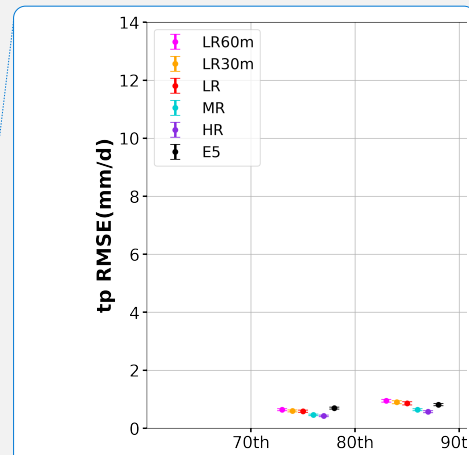
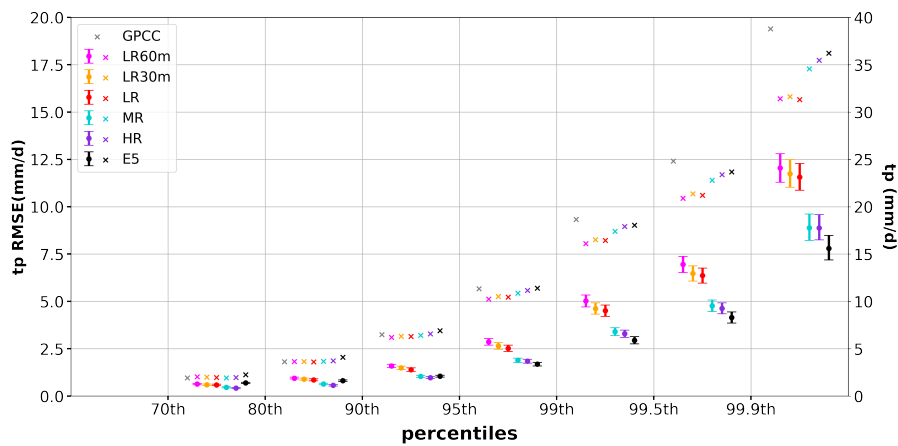
Deleted:

Deleted: c

Deleted: d

Deleted: e

Deleted: f



Deleted:

Formatted: Font: Not Bold

Formatted: Font: Not Bold

Deleted: referenced to GPCC

Formatted: English (US)

Fig. 5 European averaged precipitation amounts and RMSEs (referenced to GPCC) for European total precipitation at different percentile ranges (70th – 80th, 80th – 90th, 90th – 95th, 95th – 99th, 99th – 99.5th, 99.5th – 99.9th and >99.9th percentile) in ERA5 (black) and OpenIFS simulations (LR60m: magenta, LR30m: orange, LR: red, MR: blue, HR: purple) during 1982-2019. Cross marks are the precipitation amounts. Dots are the RMSE values, and error bars are the 95 % CI.

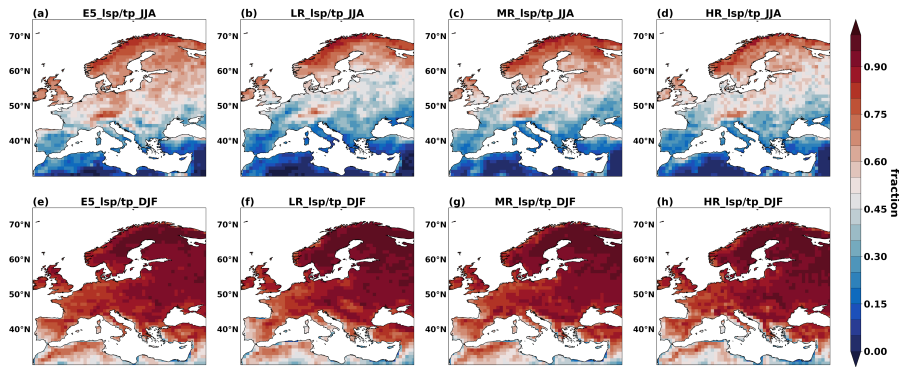
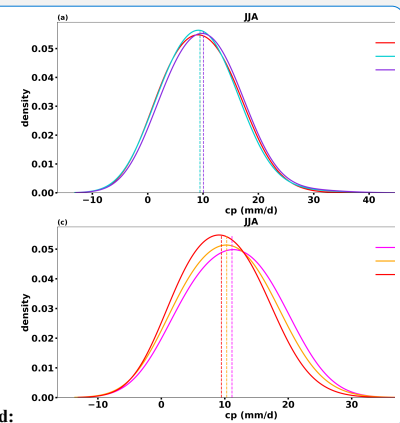


Fig. 6 Contribution of large-scale precipitation to extreme precipitation (>99th percentile) in ERA5 (a & e), LR (b & f), MR (c & g) and HR (d & h) over Europe in JJA (a-d) and DJF (e-h) over the period 1982-2019.



Deleted:

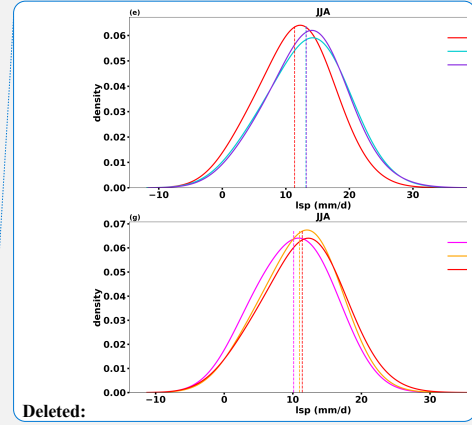
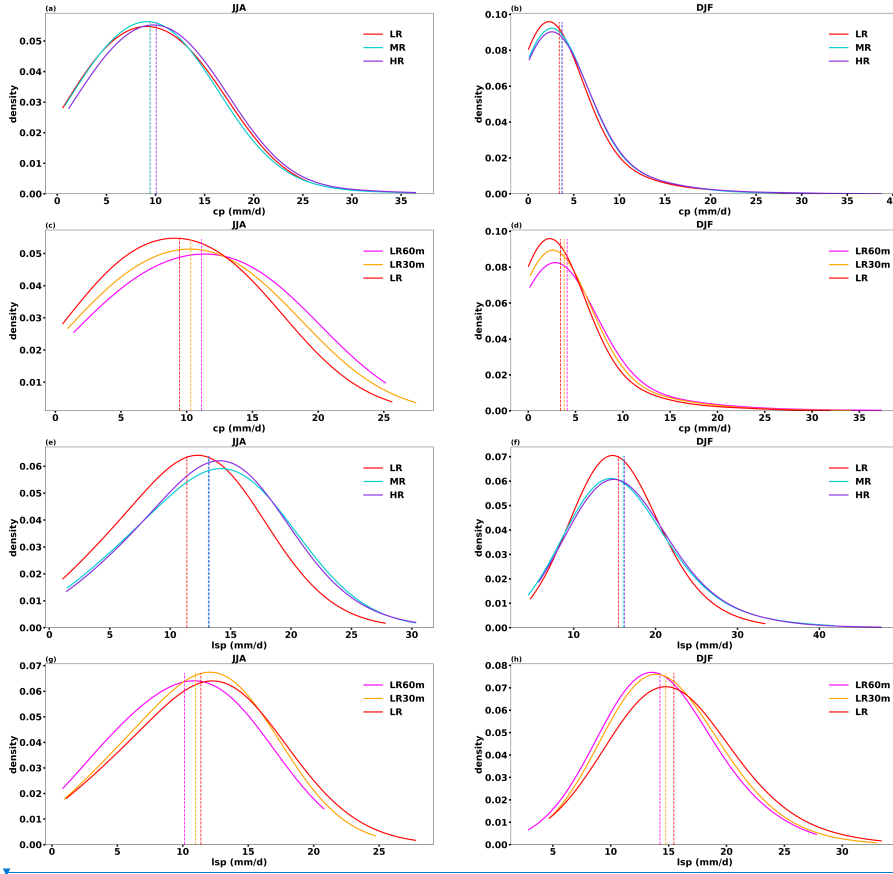


Fig. 7 European convective (a-d) and large-scale precipitation (e-h) distribution across different horizontal resolutions (a, b, e and f) and model time steps (c, d, g and h) during extreme precipitation days in JJA and DJF (LR60m: magenta, LR30m: orange, LR: red, MR: blue, HR: purple). The time period is 1982-2019. The dash lines are the mean values of each distribution.

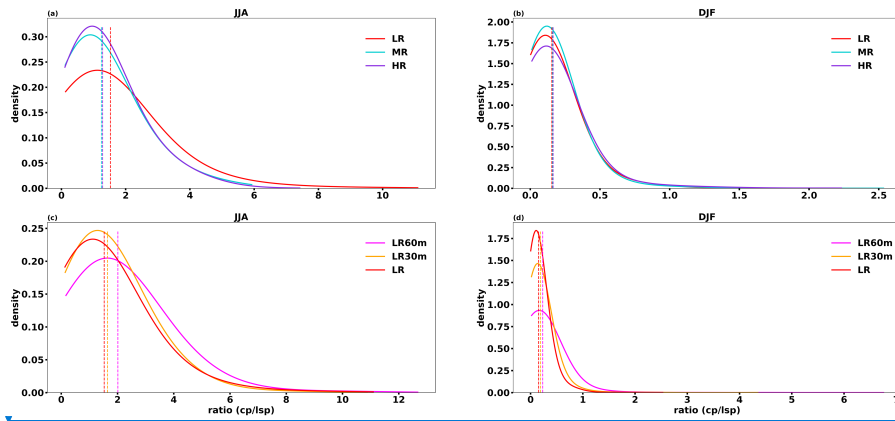


Fig. 8 The ratio between European convective and large-scale precipitation during extreme precipitation days across different horizontal resolutions (a & b) and model time steps (c & d) in JJA and DJF (LR60m: magenta, LR30m: orange, LR: red, MR: blue, HR: purple). The dash lines are the mean values of each distribution.

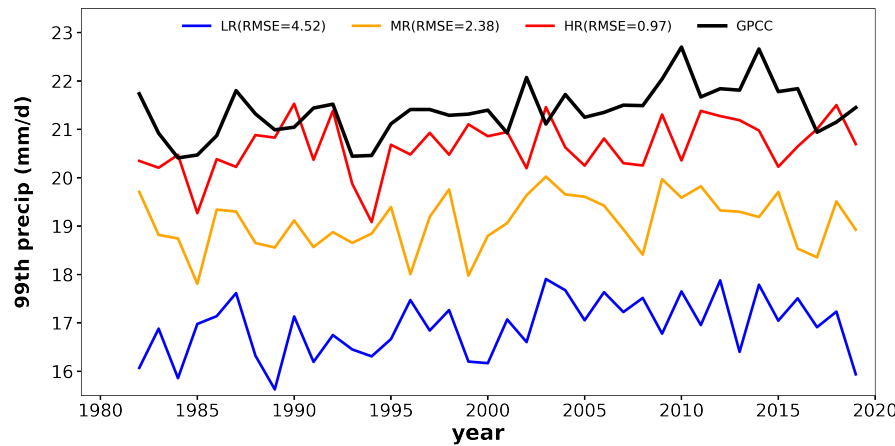


Fig. 9 Annual time series of the 99th percentile precipitation using observations (GPCC, black solid line) and model simulations on their native resolution (LR: blue, MR: orange, HR: red) during 1982-2019 over Europe. RMSE values of 99th percentile precipitation are computed referenced to GPCC which are shown within the small bracket (unit: mm/d).

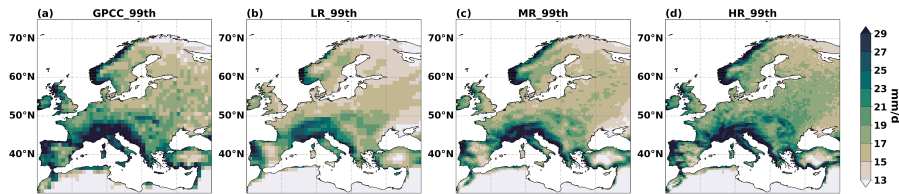


Fig. 10 The 99th percentile precipitation over Europe during 1982-2019 from (a) GPCP observations, (b) LR, (c) MR, (d) HR on their native resolution.

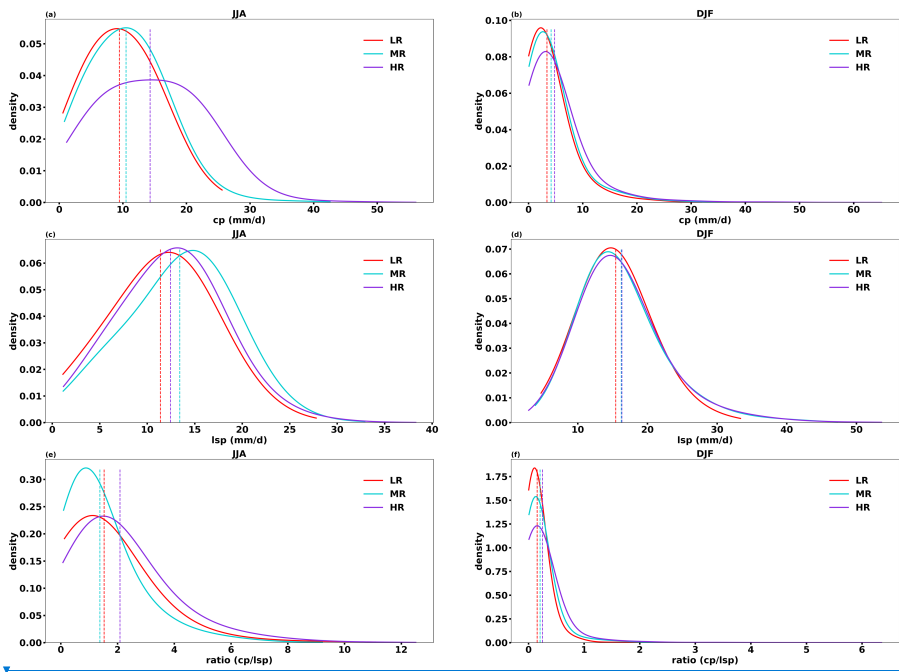
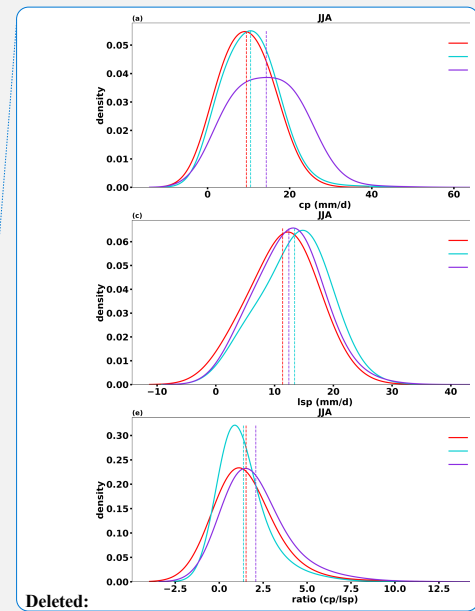


Fig. 11 European convective (a & b), large-scale precipitation (c & d) distribution and ratio (cp/lsp) on their native resolution across different horizontal resolutions during extreme precipitation days in JJA and DJF (LR: red, MR: blue, HR: purple). The time period is 1982-2019. The dash lines are the mean values of each distribution.



1028
1029
1030
1031
1032
1033
1034
1035
1036
1037
1038
1039
1040
1041
1042
1043
1044

Table 1: The experiment details of different horizontal resolutions and model time steps in OpenIFS.

Deleted: Coarsened

1046

1047 Table 2: The p-values of t-test for convective (Table 2a), large-scale precipitation (Table 2b)
1048 and their ratios (Table 2c) distribution across horizontal resolutions and model time steps. The
1049 bold means significant (p-value < 0.05).

1050

Table 2a

cp	JJA	DJF
LR → MR	0.92	0.02
MR → HR	2.1 e-4	0.75
LR60m → LR30m	4.3 e-6	0.02
LR30m → LR	5.1 e-7	0.001

1051

1052

Table 2b

lsp	JJA	DJF
LR → MR	1.8 e-29	2.2 e-4
MR → HR	0.70	0.39
LR60m → LR30m	3.3 e-9	9.4 e-5
LR30m → LR	0.005	3.0 e-7

1053

1054

Table 2c

ratio	JJA	DJF
LR → MR	3.0 e-8	0.49
MR → HR	0.37	0.64
LR60m → LR30m	1.6 e-10	9.0 e-4
LR30m → LR	0.03	2.0 e-4

1055

1056

1057

1058

1059

1060

1061

1062

1063

1064

1065

1066

